A NOVEL PRICING METHOD FOR EUROPEAN OPTIONS BASED ON FOURIER-COSINE SERIES EXPANSIONS

F. FANG* AND C.W. OOSTERLEE†

Abstract. Here we develop an option pricing method for European options based on the Fourier-cosine series, and call it the COS method. The key insight is in the close relation of the characteristic function with the series coefficients of the Fourier-cosine expansion of the density function. In most cases, the convergence rate of the COS method is exponential and the computational complexity is linear. Its range of application covers different underlying dynamics, including Lévy processes and Heston stochastic volatility model, and various types of option contracts. We will present the method and its applications in two separate parts. The first one is this paper, where we deal with European options in particular. In a follow-up paper we will present its application to options with early-exercise features.

Key words. option pricing, European options, Fourier-cosine expansion

AMS subject classifications. 65T40, 42A10, 60E10, 62P05, 91B28

Preferred short title : Cosine expansions for option pricing

1. Introduction.

Efficient numerical methods are required to rapidly price complex contracts and calibrate various financial models.

In option pricing, it is the famous Feynman-Kac theorem that relates the conditional expectation of the value of a contract payoff function under the risk-neutral measure to the solution of a partial differential equation. In the research areas covered by this theorem, various numerical pricing techniques can be developed. In brief, existing numerical methods can be classified into three major groups: partial-(integro) differential equation (PIDE) methods, monte Carlo simulation and numerical integration methods. Each of them has its merits and demerits for specific applications in finance, but the methods from the latter class are often used for calibration purposes. An important aspect of research in computational finance is to further increase the performance of the pricing methods.

State-of-the-art numerical integration techniques have in common that they rely on a transformation to the Fourier domain [7, 19]. The Carr-Madan method [7] is one of the best known examples of this class. The probability density function appears in the integration in the original pricing domain, which is not known for many relevant pricing processes. However, its Fourier transform, the characteristic function, is often available, for example from the Lévy-Khinchine theorem for underlying Lévy processes or by other means, as for the Heston model. In the Fourier domain it is possible to solve various derivative contracts, as long as the characteristic function is available. By means of the Fast Fourier Transform (FFT), integration can be performed with a computational complexity of $O(N \log_2 N)$, where N represents the number of integration points. The computational speed, especially for plain vanilla options, makes the integration methods state-of-the-art for calibration at financial institutions.

Quadrature rule based techniques are, however, not of the highest efficiency when solving Fourier transformed integrals. As the integrands are highly oscillatory, a relatively fine grid has to be used for satisfactory accuracy with the FFT.

In this paper we will focus on *Fourier-cosine expansions* in the context of numerical integration as an alternative for the methods based on the FFT. We will show that this novel method, called the COS method, can further improve the speed of

---

[*] Delft University of Technology, Delft Institute of Applied Mathematics, Delft, the Netherlands, email: f.fang@ewi.tudelft.nl,

[†] CWI – Centrum Wiskunde & Informatica, Amsterdam, the Netherlands, email: c.w.oosterlee@cwi.nl, and Delft University of Technology, Delft Institute of Applied Mathematics.

pricing plain vanilla and some exotic options. In fact, we can price a vector of strike prices simultaneously with the COS method (similar to Carr-Madan's method). Its application to American-style products will be covered in a follow-up paper. It is due to the impressive speed reported here for the COS method that we devote a paper to the European-style products. Furthermore, it offers a highly efficient way to recover the density from the characteristic function, which is of importance for several financial applications, like calibration, the computation of forward starting options, or static hedging.

This paper is organized as follows. In Section 2, we introduce the Fourier-cosine expansion for solving inverse Fourier integrals. Based on this, we derive, in Section 3, the formulas for pricing European options and the Greeks. We focus on the Lévy and Heston price processes for the underlying. An error analysis is presented in Section 4 and numerical results are given in Section 5.

2. Fourier Integrals and Cosine Series. The point-of-departure for pricing European options with numerical integration techniques is the risk-neutral valuation formula:

$$v(x,t_0) = e^{-r\Delta t}\mathbb{E}^{\mathbb{Q}}\left[v(y,T)|x\right] = e^{-r\Delta t}\int_{\mathbb{R}} v(y,T)f(y|x)dy, \qquad (1)$$

where v denotes the option value, Δt is the difference between the maturity, T, and the initial date, t_0, and $\mathbb{E}^{\mathbb{Q}}[\cdot]$ is the expectation operator under risk-neutral measure $\mathbb{Q}$. x and y are state variables at time t_0 and T, respectively; $f(y|x)$ is the probability density of y given x, and r is the risk-neutral interest rate.

In the state-of-the-art Carr-Madan approach [7], the Fourier transform of a version of valuation formula (1) is taken with respect to the log-strike price. Damping of the payoff is then necessary as, for example, a call option is not L^1-integrable with respect to the logarithm of the strike price. The method's accuracy depends on the correct value of the damping parameter. A closed-form expression for the resulting integral is available in Fourier space. To return to the time domain, quadrature rules have to be applied to the inverse Fourier integral for which the application of the FFT algorithm is appropriate.

The range of applications of numerical integration methods in finance has recently been increased by the presentation of efficient techniques for options with early exercise features [7, 19, 2, 3, 17]. Especially the CONV method [17] achieves almost linear complexity, also with the help of the FFT algorithm, for Bermudan and American options. This method can also be efficiently used for European options and numerical experiments in [17] show that the accuracy is not influenced by the choice of the damping parameter. The difference with the Carr-Madan approach is that the transform is with respect to the log-spot price in the CONV method instead of the log-strike price (something which [16] and [21] also consider). In the derivation of the CONV method the risk-neutral valuation formula is rewritten as a cross-correlation between the option value and the transition density. The cross-correlation is handled numerically by replacing the option value by its Fourier-series expansion so that the cross-correlation is transformed to an inner product of series coefficients. The coefficients are recovered by applying quadrature rules, combined with the FFT algorithm. Error analysis and experimental results have demonstrated second order accuracy and $O(N\log(N))$ computational complexity for European options.

These numerical integration methods have to numerically solve certain forward or the inverse[1] Fourier integrals. The density and its characteristic function is an example of a Fourier pair.

---

[1] Here we use the convention of the Fourier transform definition often seen in the financial engineering literature. Other conventions can also be used and modifications to the methods are then straightforward.

$$\phi(\omega) = \int_{\mathbb{R}} e^{ix\omega} f(x) dx, \tag{2}$$

$$f(x) = \frac{1}{2\pi} \int_{\mathbb{R}} e^{-i\omega x} \phi(\omega) d\omega. \tag{3}$$

Existing numerical integration methods in finance typically compute Fourier integrals by applying equally spaced numerical integration rules on the integrals, then employing the FFT algorithm by imposing the Nyquist relation to the grid sizes in the x- and ω-domains,

$$\Delta x \cdot \Delta \omega \equiv 2\pi / N,$$

with N representing the number of grid points. The grid values can then be obtained in $O(N \log_2 N)$ operations. However, there are three disadvantages: The error convergence of equally spaced integration rules, except for the Clenshaw-Curtis rule, is not very high; N has to be a power of two; finally, the relation imposed on the grid sizes prevents one from using coarse grids in both domains.

Remark 2.1. *In principle we could use the Fractional FFT algorithm (FrFT), which does not require the Nyquist relation to be satisfied, as in [8]. However, numerical tests for several options indicated that this advantage of the FrFT did not outweigh the speed of the FFT in general.*

Remark 2.2. *Alternative methods for the forward Fourier integral, based on replacing $f(x)$ in (2) by its Chebyshev [20] or Legendre [12] polynomial expansion, can achieve a high accuracy with only a limited number of terms in the expansion. However, the resulting computational complexity is typically at least quadratic.*

2.1. Inverse Fourier Integral via Cosine Expansion. In this section, as a first step, we present a different methodology for solving, in particular, the inverse Fourier integral in (3). The main idea is to reconstruct the whole integral – not just the integrand – from its Fourier-cosine series expansion (also called 'cosine expansion'), extracting the series coefficients directly from the integrand. Fourier-cosine series expansions usually give an optimal approximation of functions with a finite support[2] [5]. In fact, the cosine expansion of $f(x)$ in x equals the Chebyshev series expansion of $f(\cos^{-1}(t))$ in t.

For a function supported on $[0, \pi]$, the cosine expansion reads

$$f(\theta) = {\sum_{k=0}^{\infty}}' A_k \cdot \cos(k\theta) \quad \text{with} \quad A_k = \frac{2}{\pi} \int_0^{\pi} f(\theta) \cdot \cos(k\theta) d\theta, \tag{4}$$

where $\sum'$ indicates that the first term in the summation is weighted by one-half. For functions supported on any other finite interval, say $[a, b] \in \mathbb{R}$, the Fourier-cosine series expansion can easily be obtained via a change of variables:

$$\theta := \frac{x-a}{b-a}\pi; \quad x = \frac{b-a}{\pi}\theta + a.$$

It then reads

$$f(x) = {\sum_{k=0}^{\infty}}' A_k \cdot \cos\left(k \cdot \frac{x-a}{b-a}\pi\right), \tag{5}$$

---

[2] The usual Fourier series expansion is actually superior when a function is periodic.

with

$$A_k = \frac{2}{b-a}\int_a^b f(x) \cdot \cos(k \cdot \frac{x-a}{b-a}\pi)dx. \tag{6}$$

Since any real function has a cosine expansion when it is finitely supported, the derivation starts with a truncation of the infinite integration range in (3). Due to the conditions for the existence of a Fourier transform, the integrands in (3) have to decay to zero at ±∞ and we can truncate the integration range in a proper way without losing accuracy.

Suppose $[a, b] \in \mathbb{R}$ is chosen such that the truncated integral approximates the infinite counterpart very well, i.e.

$$\phi_1(\omega) := \int_a^b e^{i\omega x} f(x)dx \approx \int_{\mathbb{R}} e^{i\omega x} f(x)dx = \phi(\omega). \tag{7}$$

By subscripts for variables, like i in ϕ_i, we denote subsequent numerical approximations (not to be confused with subscripted series coefficients, A_k and F_k).

Comparing equation (7) with the cosine series coefficients of $f(x)$ on $[a, b]$ in (6), we find that

$$A_k \equiv \frac{2}{b-a}\mathrm{Re}\left\{\phi_1\left(\frac{\mathrm{k}\pi}{\mathrm{b-a}}\right) \cdot \exp\left(-\mathrm{i}\frac{\mathrm{ka}\pi}{\mathrm{b-a}}\right)\right\}, \tag{8}$$

where $\mathrm{Re}\{\cdot\}$ denotes taking the real part of the argument. It then follows from (7) that $A_k \approx F_k$ with

$$F_k \equiv \frac{2}{b-a}\mathrm{Re}\left\{\phi\left(\frac{\mathrm{k}\pi}{\mathrm{b-a}}\right) \cdot \exp\left(-\mathrm{i}\frac{\mathrm{ka}\pi}{\mathrm{b-a}}\right)\right\}. \tag{9}$$

We now *replace* A_k by F_k in the series expansion of $f(x)$ on $[a, b]$, i.e.

$$f_1(x) \approx {\sum_{k=0}^{\infty}}' F_k \cos\left(k\pi\frac{x-a}{b-a}\right), \tag{10}$$

and truncate the series summation such that

$$f_2(x) \approx {\sum_{k=0}^{N-1}}' F_k \cos\left(k\pi\frac{x-a}{b-a}\right). \tag{11}$$

The resulting error in $f_2(x)$ consists of two parts: a series truncation error from (10) to (11) and an error originating from the approximation of A_k by F_k. An error analysis that takes these different approximations into account is presented in Section 4.

Since the cosine series expansion of *entire functions* (i.e., functions without any singularities[3] anywhere in the complex plane, except at ∞) exhibits an *exponential convergence* [5], we can expect (11) to give highly accurate approximations to functions that have no singularities on $[a, b]$, with a small N.

To demonstrate this, we here evaluate equation (11), where

$$f(x) = \frac{1}{\sqrt{2\pi}}e^{-\frac{1}{2}x^2},$$

and determine the accuracy for different values of N. We choose $[a, b] = [-10, 10]$ and the maximum error is measured at $x = \{-5, -4, \cdots, 4, 5\}$.

Table 1 indicates that a very small error is obtained with only a small number of terms, N, in the expansion.

This technique is highly efficient for the recovery of the density function, see also Section 5.

---

[3] By 'singularity' we mean [5] poles, fractional powers, logarithms, other branch points and discontinuities in a function or in any of its derivatives.

Table 1
Maximum error when recovering $f(x)$ from $\phi(\omega)$ by Fourier-cosine expansion.

N	4	8	16	32	64
error	0.0499	0.0248	0.0014	3.50e-08	8.33e-17
cpu time (sec.)	0.0025	0.0028	0.0025	0.0031	0.0032

3. Pricing European Options. In this section, we derive the COS formula for European-style options by replacing the density function by its Fourier-cosine series. We make use of the fact that a density function tends to be smooth and therefore only a few terms in the expansion may already give a good approximation.

Since the density rapidly decays to zero as $y \to \pm\infty$ in (1), we truncate the infinite integration range without loosing significant accuracy to $[a,b] \subset \mathbb{R}$, and we obtain approximation v_1:

$$v_1(x,t_0) = e^{-r\Delta t}\int_a^b v(y,T) f(y|x) dy. \tag{12}$$

Any $[a,b]$ that covers $[x-10\sigma, x+10\sigma]$ is often sufficiently large, with σ denoting the standard deviation of the density. In the case of fat tailed distributions, which we also consider in this paper, we need larger domains.

In the second step, since $f(y|x)$ is usually not known whereas the characteristic function is, we replace the density by its cosine expansion in y,

$$f(y|x) = {\sum_{k=0}^{+\infty}}' A_k(x) \cos\left(k\pi \frac{y-a}{b-a}\right) \tag{13}$$

with

$$A_k(x) := \frac{2}{b-a}\int_a^b f(y|x)\cos\left(k\pi\frac{y-a}{b-a}\right) dy. \tag{14}$$

So that

$$v_1(x,t_0) = e^{-r\Delta t}\int_a^b v(y,T) {\sum_{k=0}^{+\infty}}' A_k(x)\cos\left(k\pi\frac{y-a}{b-a}\right) dy. \tag{15}$$

We interchange the summation and integration, and insert the definition

$$V_k := \frac{2}{b-a}\int_a^b v(y,T)\cos\left(k\pi\frac{y-a}{b-a}\right) dy, \tag{16}$$

resulting

$$v_1(x,t_0) = \frac{1}{2}(b-a)\cdot e^{-r\Delta t}\cdot {\sum_{k=0}^{+\infty}}' A_k(x)\cdot V_k. \tag{17}$$

Note that the V_k are the cosine series coefficients of $v(y,T)$ in y. Thus, from (12) to (17) we have transformed the inner product of two real functions, $f(y|x)$ and $v(y,T)$, to that of their Fourier-cosine series coefficients.

Due to the rapid decay rate of these coefficients, we further truncate the series summation to obtain approximation v_2:

$$v_2(x,t_0) = \frac{1}{2}(b-a)\cdot e^{-r\Delta t}\cdot {\sum_{k=0}^{N-1}}' A_k(x)\cdot V_k. \tag{18}$$

Similar to Section 2, coefficients $A_k(x)$ defined in (14) can be approximated by $F_k(x)$ as defined in (9). Replacing $A_k(x)$ in (18) by $F_k(x)$, we finally obtain

$$v(x,t_0) \approx v_3(x,t_0) = e^{-r\Delta t}{\sum_{k=0}^{N-1}}' \mathrm{Re}\left\{\phi\left(\frac{\mathrm{k}\pi}{\mathrm{b-a}};\mathrm{x}\right)\mathrm{e}^{-\mathrm{ik}\pi\frac{\mathrm{a}}{\mathrm{b-a}}}\right\}\mathrm{V_k}, \tag{19}$$

the COS formula for pricing European-style options. We will subsequently show that the V_k can be obtained analytically for plain vanilla and digital options.

3.1. Coefficients V_k for Plain Vanilla Options.

Before we can use (19) for pricing options, the payoff series coefficients, V_k, have to be recovered. We can find analytic solutions for V_k for several contracts.

As we assume here that the characteristic function of the log-asset price is known, we represent the payoff as a function of the log-asset price. Let us denote the log-asset prices by

$$x := \ln(S_0/K) \quad \text{and} \quad y := \ln(S_T/K),$$

with S_t denoting the underlying price at time t and K the strike price. The payoff functions for European options, in log-asset prices, read

$$v(y,T) \equiv [\alpha \cdot K(e^y - 1)]^+ \quad \text{with} \quad \alpha = \begin{cases} 1 & \text{for call,} \\ -1 & \text{for put.} \end{cases}$$

Before deriving V_k from its definition in (16), we need two mathematical entities.

Result 3.1. *The cosine series coefficients, χ_k, of $g(y) = e^y$ on $[c,d] \subset [a,b]$,*

$$\chi_k(c,d) := \int_c^d e^y \cos\left(k\pi \frac{y-a}{b-a}\right) dy, \tag{20}$$

and the cosine series coefficients, ψ_k, of $g(y) = 1$ on $[c,d] \subset [a,b]$,

$$\psi_k(c,d) := \int_c^d \cos\left(k\pi \frac{y-a}{b-a}\right) dy. \tag{21}$$

are known analytically.

Proof. Basic calculus shows that

$$\begin{aligned}\chi_k(c,d) := \frac{1}{1+\left(\frac{k\pi}{b-a}\right)^2} \Bigg[&\cos\left(k\pi\frac{d-a}{b-a}\right)e^d - \cos\left(k\pi\frac{c-a}{b-a}\right)e^c \\ &+ \frac{k\pi}{b-a}\sin\left(k\pi\frac{d-a}{b-a}\right)e^d - \frac{k\pi}{b-a}\sin\left(k\pi\frac{c-a}{b-a}\right)e^c\Bigg]\end{aligned} \tag{22}$$

and

$$\psi_k(c,d) := \begin{cases} \left[\sin\left(k\pi\frac{d-a}{b-a}\right) - \sin\left(k\pi\frac{c-a}{b-a}\right)\right]\frac{b-a}{k\pi} & k \neq 0, \\ (d-c) & k = 0. \end{cases} \tag{23}$$

□

Focusing, for example, on a call option, we obtain

$$V_k^{call} = \frac{2}{b-a}\int_0^b K(e^y - 1)\cos\left(k\pi\frac{y-a}{b-a}\right)dy = \frac{2}{b-a}K\left(\chi_k(0,b) - \psi_k(0,b)\right), \tag{24}$$

where χ_k and ψ_k are given by (22) and (23), respectively. Similarly, for a vanilla put, we find

$$V_k^{put} = \frac{2}{b-a}K\left(-\chi_k(a,0) + \psi_k(a,0)\right). \tag{25}$$

Analytic expressions of V_k can also be obtained for some exotic options.

3.2. Coefficients V_k for Digital and Gap Options. Whereas for European products equation (19) always applies, the coefficients V_k are different for different payoff functions. With analytical expressions for these coefficients, the convergence of the COS does not depend on the continuity of the payoff. For those contracts for which the V_k can only be obtained numerically, the error convergence is dominated by the numerical rules employed to determine them.

Digital options are popular in the financial markets for hedging and speculation. They are also important to financial engineers as building blocks for constructing more complex option products. Here, we consider the payoff of a cash-or-nothing call option as an example, which is 0 if $S_T \leq K$ and K if $S_T > K$. For this contract the 'cash-or-nothing call' coefficients, V_k^{cash}, can be obtained analytically:

$$V_k^{cash} = \frac{2}{b-a} K \int_0^b \cos\left(k\pi \frac{y-a}{b-a}\right) dy = \frac{2}{b-a} K \psi_k(0,b).$$

We also give the formula for a so-called gap call option [13], whose payoff reads

$$v(y,T) = [K(e^y - 1) - Rb] \cdot \mathbf{1}_{\{S_T < H\}} + Rb,$$

where $\mathbf{1}_\Psi$ equals 0 if Ψ is empty and 1 otherwise, and Rb is the so-called rebate and is paid if the barrier is hit. The time-dependent version of this payoff represents a barrier option, which will be discussed in the follow-up paper. The integral that defines V_k^{gap} for such payoff functions can be split into two parts:

$$V_k^{gap} = \frac{2}{b-a} \int_0^h K(e^y - 1) \cos\left(k\pi \frac{y-a}{b-a}\right) dy + \frac{2}{b-a} \int_h^b Rb \cdot \cos\left(k\pi \frac{y-a}{b-a}\right) dy,$$

where $h := \ln(H/K)$. It then follows that

$$V_k^{gap} = \frac{2}{b-a} K \left(\chi_k(0,h) - \psi_k(0,h)\right) + \frac{2}{b-a} Rb \cdot \psi_k(h,b). \tag{26}$$

3.3. Formula for Lévy Processes and Heston Model. Pricing formula (19) can be used for European options under any underlying process as long as the characteristic function is known. This is the case for exponential Lévy models and models from the class of regular affine processes of [11], including the exponentially affine jump-diffusion class of [10].

It is worth mentioning that (19) is simplified for the Lévy and Heston models, so that options *for many strike prices* can be computed simultaneously. For Lévy processes, whose characteristic functions can be represented by

$$\phi(\omega; x) = \varphi_{levy}(\omega) \cdot e^{i\omega x} \quad \text{with} \quad \varphi_{levy}(\omega) := \phi(\omega; 0), \tag{27}$$

the pricing formula is simplified to

$$v(x, t_0) \approx e^{-r\Delta t} {\sum_{k=0}^{N-1}}' \mathrm{Re}\left\{\varphi_{\mathrm{levy}}\left(\frac{\mathrm{k}\pi}{\mathrm{b-a}}\right) \mathrm{e}^{\mathrm{ik}\pi\frac{\mathrm{x-a}}{\mathrm{b-a}}}\right\} \mathrm{V_k}. \tag{28}$$

Recalling the V_k-formulas for vanilla European options in (24) and (25), we can represent them as $K \cdot U_k$, where

$$U_k = \begin{cases} \frac{2}{b-a}\left(\chi_k(0,b) - \psi_k(0,b)\right) & \text{for call} \\ \frac{2}{b-a}\left(-\chi_k(a,0) + \psi_k(a,0)\right) & \text{for put.} \end{cases} \tag{29}$$

As a result, the pricing formula reads

$$v(x, t_0) \approx K e^{-r\Delta t} \cdot \mathrm{Re}\left\{{\sum_{\mathrm{k}=0}^{\mathrm{N}-1}}' \varphi_{\mathrm{levy}}\left(\frac{\mathrm{k}\pi}{\mathrm{b-a}}\right) \cdot \mathrm{U_k} \cdot \mathrm{e}^{\mathrm{ik}\pi\frac{\mathrm{x-a}}{\mathrm{b-a}}}\right\}, \tag{30}$$

where the summation can be written as a matrix-vector product if K (and therefore x) is a vector. With fixed N, the computational complexity is linear in the length of vector K. In the numerical result section, we will show that with very small N one can already achieve highly accurate results.

Next, we focus on the characteristic functions and refer the reader to the literature, [9, 6, 14] for example, for background information on these processes. In particular, for the CGMY/KoBol model, which encompasses the Geometric Brownian Motion (GBM) and Variance Gamma (VG) models, the characteristic function of the log-asset price is of the form:

$$\begin{aligned}\varphi_{levy}(\omega) = \exp\left(i\omega(r-q)\Delta t - \frac{1}{2}\omega^2\sigma^2\Delta t\right)\cdot \\ \exp\left(\Delta t C\Gamma(-Y)[(M-i\omega)^Y - M^Y + (G+i\omega)^Y - G^Y]\right), \qquad (31)\end{aligned}$$

where q is a continuous dividend yield and $\Gamma(\cdot)$ represents the gamma function. In the CGMY model, the parameters should satisfy $C \geq 0, G \geq 0, M \geq 0$ and $Y < 2$. When $\sigma = 0$ and $Y = 0$ we obtain the Variance Gamma (VG) model; for $C = 0$ the Black-Scholes model is obtained.

Remark 3.1. *Note that (28) is an expression with independent variable x. It is therefore possible to obtain the option prices on different strikes in one single numerical experiment, by choosing a K-vector as the input x-vector (the same is true for the Carr-Madan formula).*

In the Heston model, the volatility, denoted by $\sqrt{u_t}$, is modeled by a stochastic differential equation,

$$\begin{aligned} dx_t &= \left(\mu - \tfrac{1}{2}u_t\right)dt + \sqrt{u_t}dW_{1t}, \\ du_t &= -\lambda(u_t - \bar{u})dt + \eta\sqrt{u_t}dW_{2t} \end{aligned} \qquad (32)$$

where x_t denotes the log-asset price variable and u_t the variance of the asset price process. Parameters $\lambda \geq 0, \bar{u} \geq 0$ and $\eta \geq 0$ are called the speed of mean reversion, the mean level of variance and the volatility of volatility, respectively. Furthermore, the Brownian motions W_{1t} and W_{2t} are assumed to be correlated with correlation coefficient ρ.

For Heston's model, the COS pricing equation is also simplified, since

$$\phi(\omega; x, u_0) = \varphi_{hes}(\omega; u_0) \cdot e^{i\omega x}, \qquad (33)$$

with u_0 the volatility of the underlying at the initial time and $\varphi_{hes}(\omega; u_0) := \phi(\omega; t_0, u_0)$. We then find

$$v(x, t_0, u_0) \approx Ke^{-r\Delta t} \cdot \mathrm{Re}\left\{ {\sum_{\mathrm{k=0}}}^{\prime\,\mathrm{N-1}} \varphi_{\mathrm{hes}}\left(\frac{\mathrm{k}\pi}{\mathrm{b-a}}; \mathrm{u_0}\right) \mathrm{e}^{\mathrm{ik}\pi\frac{\mathrm{x-a}}{\mathrm{b-a}}} \mathrm{U_k} \right\}. \qquad (34)$$

The characteristic function of the log-asset price, $\varphi_{hes}(\omega; u_0)$, reads

$$\begin{aligned}\varphi_{hes}(\omega; u_0) = \exp\left(i\omega\mu\Delta t + \frac{u_0}{\eta^2}\left(\frac{1-e^{-D\Delta t}}{2-Ge^{-D\Delta t}}\right)(\lambda - i\rho\eta\omega - D)\right)\cdot \\ \exp\left(\frac{\lambda\bar{v}}{\eta^2}\left(\Delta t(\lambda - i\rho\eta\omega - D) - 2\log\left(\frac{1-Ge^{-D\Delta t}}{1-G}\right)\right)\right),\end{aligned}$$

with

$$D = \sqrt{(\lambda - i\rho\eta\omega)^2 + (\omega^2 + i\omega)\eta^2} \quad \text{and} \quad G = \frac{\lambda - i\rho\eta\omega - D}{\lambda - i\rho\eta\omega + D}.$$

This characteristic function is uniquely specified, since we take $\sqrt{(x+yi)}$ such that its real part is nonnegative, and we restrict the complex logarithm to its principal branch. In this case the resulting characteristic function is the correct one for all complex ω in the strip of analycity of the characteristic function, as proven in [18]. Implementation of the COS formula is straightforward.

Remark 3.2 (The Greeks). *Series expansions for the Greeks, e.g.* Δ *and* Γ*, can be derived similarly. Since*

$$\Delta = \frac{\partial v}{\partial S_0} = \frac{\partial v}{\partial x}\frac{\partial x}{\partial S_0} = \frac{\partial v}{\partial x}\cdot\frac{1}{S_0}, \quad \Gamma = \frac{\partial^2 v}{\partial S_0^2} = \frac{1}{S_0^2}\left(-\frac{\partial v}{\partial S_0} + \frac{\partial^2 v}{\partial S_0^2}\right),$$

it then follows that

$$\Delta \approx e^{-r\Delta t}{\sum_{k=0}^{N-1}}{}' \mathrm{Re}\left\{\varphi\left(\frac{\mathrm{k}\pi}{\mathrm{b}-\mathrm{a}};\mathrm{u}_0\right)\mathrm{e}^{\mathrm{i}\mathrm{k}\pi\frac{\mathrm{x}-\mathrm{a}}{\mathrm{b}-\mathrm{a}}}\frac{\mathrm{i}\mathrm{k}\pi}{\mathrm{b}-\mathrm{a}}\right\}\frac{\mathrm{V}_\mathrm{k}}{\mathrm{S}_0} \tag{35}$$

and

$$\Gamma \approx e^{-r\Delta t}{\sum_{k=0}^{N-1}}{}' \mathrm{Re}\left\{\varphi\left(\frac{\mathrm{k}\pi}{\mathrm{b}-\mathrm{a}};\mathrm{u}_0\right)\mathrm{e}^{\mathrm{i}\mathrm{k}\pi\frac{\mathrm{x}-\mathrm{a}}{\mathrm{b}-\mathrm{a}}}\left[-\frac{\mathrm{i}\mathrm{k}\pi}{\mathrm{b}-\mathrm{a}} + \left(\frac{\mathrm{i}\mathrm{k}\pi}{\mathrm{b}-\mathrm{a}}\right)^2\right]\right\}\frac{\mathrm{V}_\mathrm{k}}{\mathrm{S}_0^2}. \tag{36}$$

It is also easy to obtain the formula for Vega, $\frac{\partial v}{\partial u_0}$*, for example, for Heston's model (34), as* u_0 *only appears in the coefficients:*

$$\frac{\partial v(x,t_0,u_0)}{\partial u_0} \approx e^{-r\Delta t}{\sum_{k=0}^{N-1}}{}' \mathrm{Re}\left\{\frac{\partial\varphi_{\mathrm{hes}}\left(\frac{\mathrm{k}\pi}{\mathrm{b}-\mathrm{a}};\mathrm{u}_0\right)}{\partial \mathrm{u}_0}\mathrm{e}^{\mathrm{i}\mathrm{k}\pi\frac{\mathrm{x}-\mathrm{a}}{\mathrm{b}-\mathrm{a}}}\right\}\mathrm{V}_\mathrm{k}. \tag{37}$$

4. Error Analysis.

In the derivation of the COS formula there are three steps that introduce errors: the truncation of the integration range in the risk-neutral valuation formula, the substitution of the density by its cosine series expansion on the truncated range, and the substitution of the series coefficients by the characteristic function approximation. Therefore, the overall error consists of three parts:

1. The integration range truncation error:

$$\epsilon_1 := v(x,t_0) - v_1(x,t_0) = \int_{\mathbb{R}\backslash[a,b]} v(y,T)f(y|x)dy. \tag{38}$$

2. The series truncation error on $[a,b]$:

$$\epsilon_2 := v_1(x,t_0) - v_2(x,t_0) = \frac{1}{2}(b-a)e^{-r\Delta t}\sum_{k=N}^{+\infty} A_k(x)\cdot V_k, \tag{39}$$

   where $A_k(x)$ and V_k are defined in (14) and (16), respectively.

3. The error related to approximating $A_k(x)$ by $F_k(x)$ in (9):

$$\begin{aligned}\epsilon_3 &:= v_2(x,t_0) - v_3(x,t_0)\\ &= e^{-r\Delta t}{\sum_{k=0}^{N-1}}{}' \mathrm{Re}\left\{\int_{\mathbb{R}\backslash[\mathrm{a},\mathrm{b}]}\mathrm{e}^{\mathrm{i}\mathrm{k}\pi\frac{\mathrm{y}-\mathrm{a}}{\mathrm{b}-\mathrm{a}}}\mathrm{f}(\mathrm{y}|\mathrm{x})\mathrm{d}\mathrm{y}\right\}\mathrm{V}_\mathrm{k}.\end{aligned} \tag{40}$$

We do not have to take any error in the coefficients V_k into account here, as we have a closed form solution, at least for the plain vanilla options considered in this paper.

The key to bound the errors lies in the decay rate of the cosine series coefficients. The convergence rate of the Fourier-cosine series depends on the properties of the functions on the expansion interval. We first give the definitions classifying the rate of convergence of the series for different classes of functions, taken from [5].

Definition 4.1 (Algebraic Index of Convergence). *The algebraic index of convergence* $n(\geq 0)$ *is the largest number for which*

$$\lim_{k\to\infty} |A_k|\, k^n < \infty, \qquad k >> 1,$$

where the A_k *are the coefficients of the series. An alternative definition is that if the coefficients of a series,* A_k*, decay asymptotically as*

$$A_k \sim O(1/k^n), \qquad k >> 1,$$

then n *is the algebraic index of convergence.*

Definition 4.2 (Exponential Index of Convergence). *If the algebraic index of convergence* $n(\geq 0)$ *is unbounded – in other words, if the coefficients,* A_k*, decrease faster than* $1/k^n$ *for any finite* n *– the series is said to have exponential convergence. Alternatively, if*

$$A_k \sim O(\exp(-\gamma k^r)), \qquad k >> 1,$$

with γ*, constant, the 'asymptotic rate of convergence', for some* $r > 0$*, then the series shows exponential convergence. The exponent* r *is the index of convergence.*

For $r < 1$*, the convergence is called subgeometric.*

For $r = 1$*, the convergence is either called supergeometric with*

$$A_k \sim O(k^{-n} \exp(-(k/j) \ln(k))),$$

(for some $j > 0$*), or geometric with*

$$A_k \sim O(k^{-n} \exp(-\gamma k)). \tag{41}$$

The density of the GBM process is a typical function that has a geometrically converging cosine series expansion.

Proposition 4.1 (Convergence of Fourier-cosine series [5] p.70-71). *If* $g(x) \in \mathbb{C}^\infty([a,b] \subset \mathbb{R})$*, then its Fourier-cosine series expansion on* $[a,b]$ *has geometric convergence. The constant* γ *in (41) is determined by the location in the complex plane of the singularities nearest to the expansion interval. Exponent* n *is determined by the type and strength of the singularity.*

If a function $g(x)$*, or any of its derivatives, is discontinuous, its Fourier-cosine series coefficients show algebraic convergence. Integration-by-parts shows that the algebraic index of convergence,* n*, is at least as large as* n'*, with the* n'*-th derivative of* $g(x)$ *integrable.* References to the proof of this proposition are available in [5].

The following proposition further bounds the series truncation error of an algebraically converging series:

Proposition 4.2 (Series truncation error of algebraically converging series [4]). *It can be shown that the series truncation error of an algebraically converging series behaves like*

$$\sum_{k=N+1}^{\infty} \frac{1}{k^n} \sim \frac{1}{(n-1)N^{n-1}}.$$

The proof can be found in [4].

With the two propositions above, we can state the following lemmas:

Lemma 4.1. *Error* ϵ_3 *merely consists of integration range truncation errors, and can be bounded by:*

$$|\epsilon_3| < |\epsilon_1| + Q\, |\epsilon_4|\,, \tag{42}$$

where Q is some constant independent of N and

$$\epsilon_4 := \int_{\mathbb{R}\setminus[a,b]} f(y|x)dy.$$

Proof. Assuming that $f_{Y|X}$ is a real function, we rewrite (40) as

$$\epsilon_3 = e^{-r\Delta t}{\sum_{k=0}^{N-1}}' V_k \int_{\mathbb{R}\setminus[a,b]} \cos\left(k\pi\frac{y-a}{b-a}\right) f(y|x)dy.$$

After interchanging the summation and integration, we rewrite ${\sum'}_{k=0}^{N-1}$ as $\left({\sum'}_{k=0}^{+\infty} - \sum_{k=N}^{+\infty}\right)$ and replace the cosine expansion of $v(y,T)$ in y by $v(y,T)$:

$$\begin{aligned}\epsilon_3 &= e^{-r\Delta t}\int_{\mathbb{R}\setminus[a,b]}\left[v(y,T) - \sum_{k=N}^{+\infty}\cos\left(k\pi\frac{y-a}{b-a}\right)\cdot V_k\right] f(y|x)dy \\ &= \epsilon_1 - e^{-r\Delta t}\int_{\mathbb{R}\setminus[a,b]}\left[\sum_{k=N}^{+\infty}\cos\left(k\pi\frac{y-a}{b-a}\right)\cdot V_k\right] f(y|x)dy. \qquad (43)\end{aligned}$$

According to Propositions 4.1 and 4.2, the V_k show at least algebraic convergence and we can therefore bound the expression as follows,

$$\left|\sum_{k=N}^{+\infty}\cos\left(k\pi\frac{y-a}{b-a}\right)\cdot V_k\right| \le \sum_{k=N}^{+\infty}|V_k| \le \frac{Q^*}{(N-1)^{n-1}} \le Q^*, \quad \text{for } N >> 1, n \ge 1,$$

for some positive constant Q^*. It then follows from (43) that

$$|\epsilon_3| < |\epsilon_1| + Q\,|\epsilon_4|$$

with $Q := e^{-r\Delta t}Q^*$ and $\epsilon_4 := \int_{\mathbb{R}\setminus[a,b]} f(y|x)dy$, which depends on the size of $[a,b]$. ☐

Thus, two of the three error components are truncation range related. When the truncation range is sufficiently large, the overall error is dominated by ϵ_2.

Equation (39) indicates that ϵ_2 depends on both $A_k(x)$ and V_k, the series coefficients of the density and that of the payoff, respectively. We assume that the density is typically smoother than the payoff functions in finance and that the coefficients A_k decay faster than V_k. Consequently, the product of A_k and V_k converges faster than either A_k or V_k, and we can bound this product as follows,

$$\left|\sum_{k=N}^{+\infty} A_k(x)\cdot V_k\right| \le \sum_{k=N}^{+\infty}|A_k(x)|. \qquad (44)$$

Error ϵ_2 is thus dominated by the series truncation error of the density function.

PROPOSITION 4.3 (Series truncation error of geometrically converging series [5] p.48). *If a series has geometrical convergence, then the error after truncation of the expansion after $(N+1)$ terms, $E_T(N)$, reads*

$$E_T(N) \sim P^* \cdot \exp(-N\nu).$$

Here, constant $\nu > 0$ is called the asymptotic rate of convergence of the series, which satisfies

$$\nu = \lim_{n\to\infty}\left(-\log|E_T(n)|/n\right),$$

and P^* denotes a factor which varies less than exponentially with N.

Lemma 4.2. *Error ϵ_2 converges exponentially in the case of density functions $\in \mathbb{C}^\infty([a,b])$.*

$$|\epsilon_2| < P \cdot \exp(-(N-1)\nu), \tag{45}$$

where $\nu > 0$ is a constant and P is a term that varies less than exponentially with N. The proof of this is straightforward, applying Proposition 4.3 to (44).

Based on Proposition 4.2, we can prove the following lemma:

Lemma 4.3. *Error ϵ_2 for densities having discontinuous derivatives can be bounded as follows:*

$$|\epsilon_2| < \frac{\bar{P}}{(N-1)^{\beta-1}}, \tag{46}$$

where $\bar{P}$ is a constant and $\beta \geq n \geq 1$ (n the algebraic index of convergence of V_k). The proof of this lemma is straightforward. Note that $\beta \geq n$ is because the density function is usually smoother than a payoff function.

Collecting the results (38), (42), (45) and (46), we can summarize that, with a properly chosen truncation of the integration range, the overall error converges either exponentially for density functions that belong to $\mathbb{C}^\infty([a,b] \subset \mathbb{R})$, i.e.

$$|\epsilon| < 2\,|\epsilon_1| + Q\,|\epsilon_4| + Pe^{-(N-1)\nu}, \tag{47}$$

or algebraically for density functions with a discontinuity in one of its derivatives, i.e.

$$|\epsilon| < 2\,|\epsilon_1| + Q\,|\epsilon_4| + \frac{\bar{P}}{(N-1)^{\beta-1}}. \tag{48}$$

To determine the size of the truncation range as a multiple of the standard deviation of $\ln(S_T/K)$, we use a rule of thumb, from [19]:

$$b - a = L \cdot \sqrt{-\left.\frac{\partial^2 \phi(T,\omega)}{\partial \omega^2}\right|_{\omega=0} + \left(\left.\frac{\partial \phi(T,\omega)}{\partial \omega}\right|_{\omega=0}\right)^2} \tag{49}$$

where $\phi(t,\omega)$ is the characteristic function of $\ln(S_t/K)$ conditional upon $\ln(S_0/K)$, and L is a proportionality constant, which can be chosen as $L = 10$ for Gaussian density functions but should be chosen somewhat larger in the case of fat tails. The center of the expansion interval is placed at $\ln(S_0/K)$.

5. Numerical Results. In this section, we perform a variety of numerical tests to evaluate the efficiency and accuracy of the COS method. We focus on the plain vanilla European options and consider different processes for the underlying asset from geometric Brownian motion to the Heston stochastic volatility process and the infinite activity Lévy processes Variance Gamma and CGMY. In the latter case we choose a value for parameter Y close to 2, representing a distribution with very heavy tails. We will choose long and short maturities in the tests, and as a final example we will also consider a digital option.

The underlying density functions for each individual experiment are also recovered with the help of the cosine series based inverse technique presented in Section 2. This may help the reader to get some insight into the relationship between the error convergence and the properties of the densities.

We compare our results with the COS method to two of its competitors for European option pricing, the Carr-Madan method [7] and the CONV method [17]. However, contrary to the common implementations of these methods we use the

Simpson's rule for the Fourier integrals in order to achieve fourth order convergent techniques. In that case the FFT can be used for the Carr-Madan as well as for the CONV method.

REMARK 5.1. *Some experience is helpful when choosing the correct truncation range and damping factor α in Carr-Madan's method. A suitable choice appears to be $\alpha = 0.75$, for the experiments based on GBM as well as on Heston's model.*

The CONV method can be used without any form of damping for the option parameters used here.

In all experiments, we set the same truncation range of the density domain for the COS and the CONV methods. By these numerical experiments and comparisons with the other methods, we aim to demonstrate the stability and robustness of the new COS method, also under extreme conditions.

It should be noted that parameter N in the experiments to follow denotes, for the COS method, the number of terms in the Fourier-cosine expansion, and the number of grid points for the other two methods.

All CPU times presented, in milliseconds, are determined after averaging the computing times obtained from 100 experiments. The computer used for all experiments has an Intel(R) Pentium(R) 4 CPU, 2.80GHz with cache size 1024 KB; The code is written in Matlab 7-4.

5.1. Geometric Brownian Motion, GBM.

The first set of experiments are performed under the GBM process with a short time to maturity. Parameters selected for this test are

$$S_0 = 100, r = 0.1, q = 0, T = 0.1, \sigma = 0.25. \tag{50}$$

Domain length parameter in (49) $L = 10$.

The convergence behavior at three different strike prices, $K = 80, 100$ and 120, is checked. Reference values for these tests are based on an accurate adaptive integration scheme with a large number of points of the Carr-Madan formula.

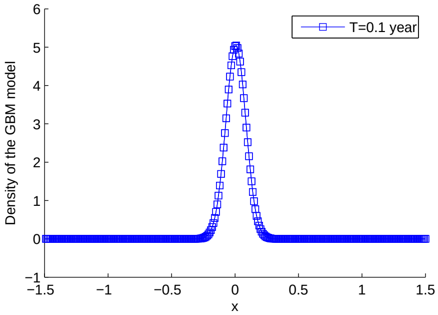

FIG. 1. *Recovered density function of the GBM model involved in the experiments; $K = 100$, other parameters as in (50).*

Figure 1 shows that the recovered density function with the small maturity time T does not have fat tails, as is commonly known. This implies that the tails of the characteristic function in the Fourier domain are fat. As a result, the truncation range for the Carr-Madan method in the Fourier domain has to be selected relatively large. Therefore, a significantly larger value of N is necessary compared to the other two methods to achieve the same level of accuracy.

As shown in Figure 2, the error convergence of the COS method is exponential (geometric) and superior to that of the 4-th order CONV and Carr-Madan methods. With $N = 2^7$, the COS results already coincide with the reference values that are

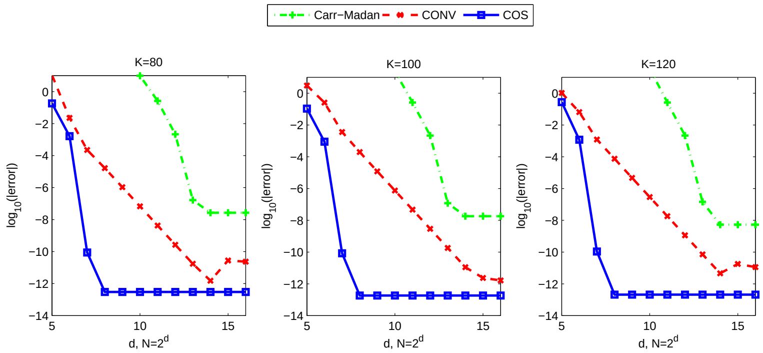

FIG. 2. *COS vs. Carr-Madan and CONV in error convergence for pricing European call options under GBM model*

12 digits accurate. Further, we observe that the error convergence rate is basically the same for the different strike prices.

Note that the results for these strikes are obtained in one single numerical experiment by the COS and the Carr-Madan method. In Table 2, cpu time and error convergence information, comparing the COS and the Carr-Madan method, are displayed for pricing the options at $K = 80, 100$ and 120 in one computation. To get the same level of accuracy, the COS method uses significantly less cpu time; this becomes more prominent when the desired accuracy is high. For the Carr-Madan computation we have used a truncation range of size $[0, 100]$ in this latter experiment [4]

REMARK 5.2. *We have observed a linear computational complexity for the COS method by doubling N and performing the computations. This cannot be observed in Table 2, as the biggest portion of time spent on the experiments with relatively small N is computational overhead.*

TABLE 2
Error convergence and cpu time comparing the COS and Carr-Madan methods for European options under GBM, parameters as in (50), and $K = 80, 100, 120$.

	N	32	64	128	256	512
COS	msec	0.0401	0.0519	0.0763	0.2532	0.4634
	max. error	1.98e-01	4.62e-04	5.55e-11	2.77e-13	2.77e-13
Carr-Madan	msec	0.2824	0.2749	0.3101	0.7013	1.0596
	max. error	6.85e+05	2.09e+02	1.11e+00	7.57e-02	3.57e-03

5.1.1. Cash-or-nothing Option. We confirm that the convergence of the COS method does not depend on a discontinuity in the payoff function, provided we have an analytic expression for the coefficients V_k^{cash} by pricing a cash-or-nothing call option here. The underlying process is GBM, so that an analytic solution exists. Parameters selected for this test are

$$S_0 = 100, K = 120, r = 0.05, q = 0, T = 0.1, \sigma = 0.2, L = 10. \tag{51}$$

Table 3 presents the exponential convergence of the COS method.

---

[4] To produce the Carr-Madan results from Figure 2 with very small errors, we needed a larger truncation range, i.e., $[0, 1200]$.

Table 3

Error and cpu time for a cash-or-nothing call option with the COS method, parameters as in (51); Reference $v(0, 90) = 0.27330649649\ldots$

N	40	60	80	100	120	140
error	2.46e-02	1.64e-02	6.35e-04	6.85e-06	2.44e-08	2.79e-11
cpu time (msec.)	0.0330	0.0334	0.0376	0.0428	0.0486	0.0497

5.2. Heston Model. As a second test we choose the Heston model with the following parameters:

$$\begin{aligned} &S_0 = 100, K = 100, r = 0, q = 0, \lambda = 1.5768, \eta = 0.5751, \\ &\bar{u} = 0.0398, u_0 = 0.0175, \rho = -0.5711. \end{aligned} \tag{52}$$

Two maturity dates are chosen and the length of the domain L is set accordingly. We evaluate $T = 1$ with $L = 10$ and $T = 10$ with $L = 30$.

In (49) we need to compute the standard deviation of the Heston model, which can be approximated well by the quantity $\sqrt{\bar{u} + \bar{u}\eta}$. Figure 3 presents the recovered density functions. It shows that $T = 10$ gives rise to fatter tails in the density function, as expected.

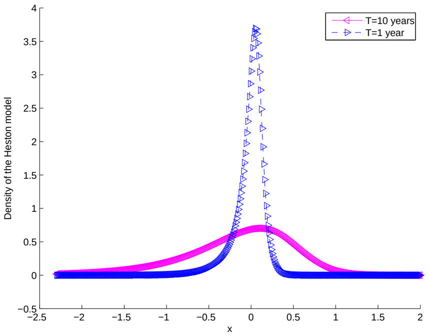

Fig. 3. *Recovered density functions of the Heston experiments, parameters as in (52).*

In this test we compare the COS method with the Carr-Madan method, which is state-of-the-art for the calibration of Heston model in industry. The truncated Fourier domain for the Carr-Madan method is set to $[0, 1200]$ for the experiment with $T = 1$, and to $[0, 500]$ for $T = 10$. The option price reference values are obtained by the Carr-Madan method using $N = 2^{18}$ points. We find $v(S_0, 0) = 5.785155435\ldots$ for $T = 1$ and $v(S_0, 0) = 22.318945791474590$ for $T = 10$.

Tables 4 and 5 illustrate the high efficiency of the COS method as compared to the Carr-Madan method.

Note that all times are given in milli-seconds. The COS method, however, appears to be approximately a factor 20 faster than the Carr-Madan method. The convergence rate of the COS method is somewhat slower for the short maturity example, as compared to for the 10 years maturity. This is due to the fact that the density function for the latter case is smoother, as seen in Figure 3. The COS convergence rate for small T is, however, still exponential in Heston model.

Additionally, for a fair comparison, we mimic the calibration situation, in which around 20 strikes are priced simultaneously. We repeat the experiment for $T = 1$ but now with 21 consecutive strikes, $K = 50, 55, 60, \cdots, 150$, see the results in Table 6. With $N = 200$, the COS method can price all options for 21 strikes highly accurately, within 0.5 milli-seconds.

Table 4

Error convergence and cpu times for the COS and Carr-Madan methods for the Heston model with $T = 1$, parameters as in (52).

COS			Carr-Madan		
N	error	time (msec.)	N	error	time (msec.)
40	4.69e-02	0.0607	512	1.79e+06	0.6702
80	3.81e-04	0.0805	1024	2.16e+01	1.1874
120	1.17e-05	0.1078	2048	2.61e-01	1.9373
160	6.18e-07	0.1300	4096	2.15e-03	3.5577
200	3.70e-09	0.1539	8192	1.40e-07	7.5376

Table 5

Error convergence and cpu time for the COS and Carr-Madan methods for the Heston model with $T = 10$, parameters as in (52).

COS			Carr-Madan		
N	error	time (msec.)	N	error	time (msec.)
40	4.96e-01	0.0598	512	3.27e+01	1.2260
65	4.63e-03	0.0747	1024	2.61e-01	1.1872
90	1.35e-05	0.0916	2048	2.15e-03	2.0237
115	1.08e-07	0.1038	4096	1.11e-07	3.8807
140	9.88e-10	0.1230	8192	2.70e-08	7.5381

Table 6

Error convergence and cpu time for the Heston model by the COS and Carr-Madan method, pricing 21 strikes, with $T = 1$, parameters as in (52).

COS	N	40	80	160	200
	cpu time (msec.)	0.1015	0.1766	0.3383	0.4214
	max. error	0.0519	7.18e-04	6.18e-07	2.05e-08
Carr-Madan	N	1024	2048	4096	8192
	cpu time (msec.)	1.1043	2.1199	3.8137	7.3551
	max. error	66.8768	0.2608	0.0021	2.0825e-07

5.3. Variance Gamma, VG. As a next example we price options under the Variance Gamma process, which belongs to the class of infinite activity Lévy processes. The VG process is usually parameterized with parameters σ, θ and ν related to C, G and M in (31) through

$$C = \frac{1}{\nu},\ G = \frac{\theta}{\sigma^2} + \sqrt{\frac{\theta^2}{\sigma^4} + \frac{2}{\nu\sigma^2}},\ M = -\frac{\theta}{\sigma^2} + \sqrt{\frac{\theta^2}{\sigma^4} + \frac{2}{\nu\sigma^2}}, \tag{53}$$

The parameters selected in the numerical experiments are

$$K = 90, S_0 = 100, r = 0.1, q = 0, \sigma = 0.12, \theta = -0.14, \nu = 0.2. \tag{54}$$

This case has been chosen because a relatively slow convergence was reported for the CONV method for very short maturities in [17]. Here, we compare the convergence for $T = 1$ (with $L = 10$) and for $T = 0.1$ year (setting $L = 20$).

Figure 4 presents the difference in shape of the two recovered density functions. For $T = 0.1$, the density is much more peaked. Note that for $T = 0.1$ the error convergence of the COS method is algebraic instead of exponential. This is in agreement with the recovered density function in Figure 4, which is clearly not in $C^\infty([a, b] \subset \mathbb{R})$. In the extreme case, we would observe a delta function-like function for $T \to 0$.

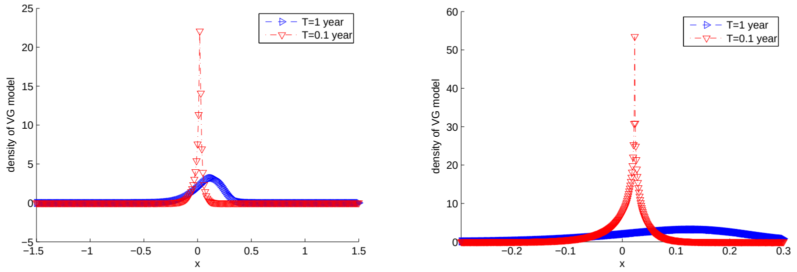

(a) Whole density function

(b) Zoom in

FIG. 4. *Recovered density functions for the VG model and two maturity dates; $K = 90$, other parameters as in (54).*

TABLE 7
Convergence of the COS method for the VG model with $K = 90$, parameters as in (54).

$T = 0.1$; Reference $v(0, 90) = 19.09935472\ldots$			$T = 1$; Reference $v(0, 90) = 10.993703186\ldots$		
N	error	time(msec.)	N	error	time(msec.)
128	5.43e-04	0.0709	30	6.08e-04	0.0379
256	7.08e-05	0.1178	60	1.89e-07	0.0473
512	3.80e-06	0.2130	90	1.60e-08	0.0592
1024	2.35e-05	0.1049	120	5.97e-10	0.0731
2048	1.41e-07	0.7809	150	3.29e-12	0.0811

We also plot the errors in Figure 5, comparing the convergence of the COS method to that of the (N^{-2})-CONV method[5]. The convergence rate of the COS method for $T = 1$ is significantly faster than that of the CONV method, but for $T = 0.1$ the convergence is comparable.

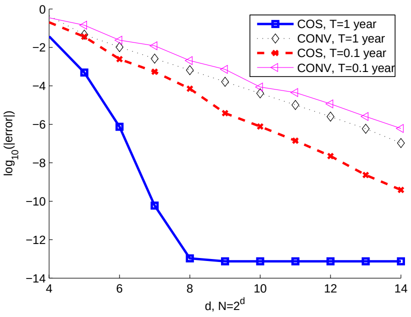

FIG. 5. *Convergence of the COS method for VG model*

5.4. CGMY Process. Finally, we evaluate the method's convergence for the CGMY model. It has been reported in [1, 22] that PIDE methods have difficulty solving the cases for which $1 \le Y \le 2$. Therefore we evaluated the COS method with $Y = 0.5$, $Y = 1.5$ and $Y = 1.98$, respectively. The other parameters are selected as follows:

$$S_0 = 100, K = 100, r = 0.1, q = 0, C = 1, G = 5, M = 5, L = 10, T = 1. \qquad (55)$$

In Figure 6, the recovered density functions for the three cases are plotted. For

---

[5] The Simpson rule did not improve the convergence rate here.

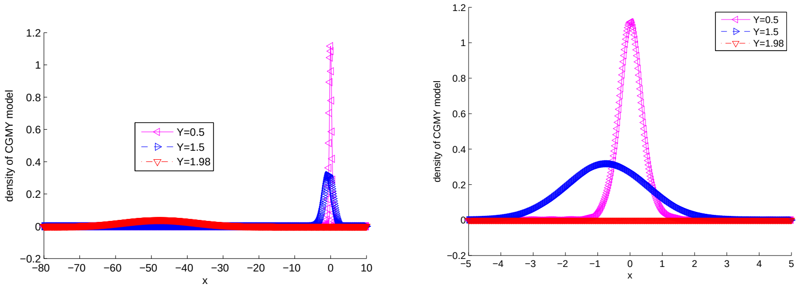

(a) Complete density functions (b) Zoom of density functions

Fig. 6. *Recovered density functions for the CGMY model with different values of Y; other parameters as in (55).*

large values of Y the tails of the density function are fatter and the center of the distribution shifts.

Therefore, we use adapted truncation ranges in this case given by $[-L \cdot Y, L \cdot Y]$ for $Y = 0.5$ and $Y = 1.5$ with $L = 10$ and the range is set to $[-100, 20]$ for $Y = 1.98$; Reference values for the numerical experiments are computed with the COS method with $N = 2^{19}$, as there are no reference values available for the latter cases. The numerical results are presented in Tables 8 and 9, for $Y = 0.5$ and $Y = 1.5$, respectively.

Table 8

Comparison of the COS and CONV methods in accuracy and speed for CGMY with $Y = 0.5$ and the other parameters from (55); Ref.val.=19.8129487706 . . .

COS			CONV		
N	error	time (msec.)	N	error	time (msec.)
40	3.82e-02	0.0560	64	2.13e-02	0.0595
60	6.87e-04	0.0645	128	6.42e-04	0.0836
80	2.11e-05	0.0844	256	3.82e-05	0.1366
100	9.45e-07	0.1280	512	2.30e-06	0.2551
120	5.56e-08	0.1051	1024	9.86e-08	0.4957
140	4.04e-09	0.1216	2048	2.93e-08	0.9893

Table 9

Comparison of the COS and CONV methods in accuracy and speed for CGMY with $Y = 1.5$ and the other parameters from (55); Ref.val.=49.790905305 . . ..

COS			CONV		
N	error	time (msec.)	N	error	time (msec.)
40	1.38e+00	0.0545	64	1.17e-02	0.0600
45	1.98e-02	0.0589	128	6.92e-04	0.0928
50	4.52e-04	0.0689	256	4.26e-05	0.1622
55	9.59e-06	0.0690	512	2.73e-06	0.2776
60	1.22e-09	0.0732	1024	3.93e-07	0.5189
65	7.53e-10	0.0748	2048	2.18e-07	0.9773

Again, the COS method converges exponentially, which is faster than the 4th order convergence of the CONV method. With a relatively small value of N, i.e. $N \leq 100$, the COS results are accurate up to 7 digits. The computational time spent is less than 0.1 millisecond. Comparing Tables 8 and 9, we notice that the convergence rate with $Y = 1.5$ is faster than that of $Y = 0.5$, as opposed to the convergence of the CONV method. Density functions from fat-tailed distributions can often be well represented by cosine basis functions.

TABLE 10

The COS method for CGMY model with $Y = 1.98$; other parameters as in (55). Reference value $= 0.252104475\ldots$

N	20	25	30	35	40
msec	0.0438	0.0463	0.0485	0.0511	0.0538
error	4.17e+02	5.15e-01	6.54e-05	1.10e-09	1.94e-15

6. Conclusions and Discussion. In this paper we have introduced an option pricing method based on Fourier-cosine series expansions, the COS method, for pricing European-style options. The method can be used as long as a characteristic function for the underlying price process is available. The COS method is based on the insight that the series coefficients of many density functions can be accurately retrieved from their characteristic functions. As such, one can decompose a density function into a linear combination of cosine functions. It is this decomposition that makes the numerical computation of the risk-neutral valuation formula easy and highly efficient.

Derivation of the COS method has been accompanied by an error analysis. In several numerical experiments, the convergence rate of the COS method has shown to be exponential, in accordance with the analysis. When the density function of the underlying process has a discontinuity in one of its derivatives an algebraic convergence is expected and was observed. The computational complexity of the COS method is linear in N, the number of terms chosen in the Fourier-cosine series expansion. Very fast computing times were reported here for the Heston and Lévy models. With $N < 150$, all numerical results obtained are accurate up to 8 digits, in less than 0.5 milliseconds of cpu time. By recovering the density function we can estimate the convergence behavior of our numerical method.

The generalization to high dimensional option pricing problems is not trivial, because an analytic formula for the coefficients V_k cannot easily be obtained. The V_k should then be recovered numerically, which has an impact on the convergence rate of the COS method. This is part of our future research.

Acknowledgments: The authors would like to thank Roger Lord (Rabobank, London) and Hans van der Weide (Delft University of Technology) for fruitful discussions.

REFERENCES

[1] Almendral A. and Oosterlee C.W., Accurate evaluation of European and American options under the CGMY process., *SIAM J. Sci. Comput.* 29: 93-117, 2007.

[2] Andricopoulos A.D., Widdicks M., Duck P.W. and Newton D.P., Universal option valuation using quadrature methods, *J. Fin. Economics,* 67: 447-471, 2003.

[3] Andricopoulos A.D., Widdicks M., Duck P.W. and Newton D.P., Extending quadrature methods to value multi-asset and complex path dependent options, *J. Fin. Economics,* 2006.

[4] Bender C.M. and Orszag S.A., *Advanced mathematical methods for scientists and engineers.* McGraw-Hill, New York, 1978.

[5] Boyd J.P., *Chebyshev & Fourier spectral methods*, Springer-Verlag, Berlin, 1989.

[6] Carr P.P., Geman H., Madan D.B. and Yor M., The fine structure of asset returns: An empirical investigation. *J. of Business,* 75: 305-332, 2002.

[7] Carr P.P. and Madan D.B., Option valuation using the fast Fourier transform. *J. Comp. Finance,* 2:61-73, 1999.

[8] Chourdakis K., Option pricing using the fractional FFT. *J. Comp. Finance* 8(2), 2004.

[9] Cont R. and Tankov P., *Financial modelling with jump processes*, Chapman and Hall, Boca Raton, FL, 2004.

[10] Duffie D., Pan J. and Singleton K., *Transform analysis and asset pricing for affine jump-diffusions.* Econometrica 68: 1343–1376, 2000.

[11] Duffie D., Filipovic D. and Schachermayer W., Affine processes and applications in finance. *Ann. of Appl. Probab.,* 13(3): 984-1053, 2003.

[12] Evans G.A. and Webster J.R., A comparison of some methods for the evaluation of highly oscillatory integrals. *J. of Comp. Applied Math.* 112: 55-69, 1999.

[13] Haug E.G., *The complete guide to option pricing formulas.* McGraw-Hill, 1998.

[14] Heston S., A closed-form solution for options with stochastic volatility with applications to bond and currency options. *Rev. Financ. Studies,* 6: 327-343, 1993.

[15] Hull J.C. *Options, futures and other derivatives.* Prentice Hall. 4th ed., 2000.

[16] Lewis A. *A simple option formula for general jump-diffusion and other exponential Lévy processes.* SSRN working paper, 2001. Available at: `http//ssrn.com/abstract=282110`.

[17] Lord R., Fang F., Bervoets F. and Oosterlee C.W., *A fast and accurate FFT-based method for pricing early-exercise options under Lévy processes.* SSRN, page http://ssrn.com/abstract=966046, 2007. To appear in SIAM J. Sci. Comput.

[18] Lord R. and Kahl Ch., *Complex logarithms in Heston-like models.* Working paper, Rabobank International and ABNAMRO, 2008. See `http://www.rogerlord.com/complexlogarithmsheston.pdf`.

[19] O'Sullivan C., *Path dependent option pricing under Lévy processes* EFA 2005 Moscow Meetings Paper, Available at SSRN: `http://ssrn.com/abstract=673424`, Febr. 2005

[20] Piessens R. and Poleunis F., A numerical method for the integration of oscillatory functions, *BIT,* 11: 317-327, 1971.

[21] Raible S., *Lévy processes in finance: Theory, numerics and empirical facts.* PhD Thesis, Inst. für Math. Stochastik, Albert-Ludwigs-Univ. Freiburg, 2000.

[22] Wang I., Wan J.W. and Forsyth P., Robust numerical valuation of European and American options under the CGMY process. *J. Computational Finance,* 10(4): 31-70, 2007.